DEVELOPMENT OF AN ELECTRON TIME OF FLIGHT SPECTROMETER FOR ULTRAFAST PULSE CHARACTERIZATION AND ULTRAFAST DYNAMICS STUDIES

by

PRATAP TIMILSINA

B.S., Tribhuvan University, Nepal, 2007
M.S., Bharathidasan University, India, 2010

A REPORT

Submitted in partial fulfillment of the requirements for the degree

MASTER OF SCIENCE

Department of Physics
College of Arts and Sciences

KANSAS STATE UNIVERSITY
Manhattan, Kansas

2016

Approved by:

Major Professor
Carlos Trallero

Copyright

Abstract

This report presents the details of an electron time-of-flight (ETOF) spectrometer to be used for characterizing ultrafast electric field pulses. The pulses will range in pulse-duration from femtosecond to attoseconds and in wavelength from the far infrared (FIR) to the extreme ultra violet (XUV). By measuring the photoelectrons in the presence of two electric fields and their quantum interference we will be able to extract the amplitude and phase of the electric field. For XUV pulses this is the well-known streaking and Reconstruction of Attosecond Beating by Interference of Two-Photon Transition (RABITT) method.

The ETOF is based on a set of tunable electrostatic lenses capable of detecting 0-150 eV electrons. In addition, we can selectively increase the photoelectron yield of the spectrum. The precise tuning of the electrostatic lens system is done with a Genetic Algorithm (GA) with an intensity fluctuation discriminator in the fitness.

Table of Contents

List of Figures

List of Tables

Acknowledgements

First of all, I would like to thank Professor Carlos Trallero for giving me the opportunity to work in his group and to involve myself in experimental physics research on Atomic Molecular and Optical physics. I would like to thank my graduate committee members: Professor Daniel Rolles and Professor Artem Rudenko.

I would like to thank all present and past group members: Giriraj Jnawali, Georgios Kolliopoulos, Stefan Zigo, Derrek Wilson, Adam Summers, Jan Tross, Brandin Davis, Wes Erbsen, Phillip Mundine and Sudipta Mondal for both research related support as well as moral support. I would like to acknowledge Prof. Itzik's group member Travis Severt with whom I was involved in one of the projects. I highly appreciate the technical support I received from Al Rankin, Mike Wells, Scott Chainey, Chris Aikens and Vince Needham.

I am thankful to all faculty members, staff and friends of the Physics Department for their support during my graduate studies. I would like to thank my friends from the Nepalese community of Manhattan who helped me from the beginning of my time in Manhattan, it was really a great moral support for me.

Dedication

This work is dedicated to my family. To my father, **Prakash Timilsina** and to my mother, **Laxmi Timilsina,** who have always been very supportive all of the time. To my elder brother **Pradeep Sharma,** for his constant guidance and for being my close and motivating friend. To my beloved wife **Sandhya Paudel Timilsina** who has been supporting me during my graduate studies.

Chapter 1 - Introduction and Background

Femtosecond laser pulses [1] when focused down to a few μm can produce peak intensities of the order 10^{12} to 10^{15} W/cm^2. or even higher. At these peak intensities, the electric field is strong enough to distort the binding potential of atoms. This distortion is the basis of strong field phenomena. Some examples of such phenomena are ionization of atoms and molecules, and high order harmonic generation (HHG). This report focuses on the development of a tool that can be used for strong field ionization and HHG studies. In particular, we are interested in the characterization of HHG radiation. This interest comes from the fact that HHG can be used as an atomic and molecular spectroscopic tool, providing a time-dependent, coherent measurement of the photoionization dipole moment. In this chapter we introduce some of the terms and the physical processes that are mentioned throughout the thesis.

1.1 Strong Field Ionization

Strong field ionization is the process in which an atom or a molecule absorbs multiple photons and one or multiple electrons are emitted. To study this process, we can either measure the emitted electrons or the remnant ions. While the instrument developed in this thesis can measure both charged particles, we will focus on the electrons. Additionally, depending on the wavelength or the intensity of the incoming radiation, the ionization process can be divided into two categories: tunneling ionization or multiphoton ionization.

1.1.1 Above Threshold Ionization

Multiphoton ionization (MPI) is the process of ionization in which several photons of energy smaller than the ionization threshold are absorbed by an atom and combine their energies to ionize the atom [Figure 1.1(a)]. Above Threshold Ionization (ATI) is an extension of multi-photon ionization in which more energy is absorbed than is necessary to ionize the atom. [2] The excess energy gives the released electron kinetic energy and for each extra photon there will be a peak in the photoelectron spectrum [Figure 1.1(b)]. Such a photoelectron spectrum is called an ATI spectrum. The electrons released from the target will have energies separated by an integer number of photon energies $\hbar\omega$ [3]. The positions of the ATI peaks are predictable by the equation,

$$E = (n+s)\hbar\omega-(I_p+U_p), \qquad (1.1)$$

where E is the electron kinetic energy, n is the number of photons needed to overcome the ionization potential, s is the number of excess photons, ω is the angular frequency of the laser field, I_p is the ionization potential and U_p is the ponderomotive energy. The ponderomotive energy is defined as the kinetic energy of an electron quivering in the laser field, averaged over an optical cycle. For the case of a linearly polarized monochromatic laser field, the non-relativistic expression for the U_p is,

$$U_p = \frac{I}{4\omega^2} \qquad (1.2)$$

where I is the peak laser intensity and ω is the angular frequency. The unit used in Eq.(1.2) are in atomic unit.

1.1.2 Tunnel Ionization

If the laser intensity is so strong ($I \geq 10^{14}$ W/cm^2) that the Coulomb potential starts to be distorted, oscillations with the external electric field occur and the electron might tunnel through the laser-induced potential barrier. This is called tunnel ionization [4] and pictured in Figure 1.1(c).

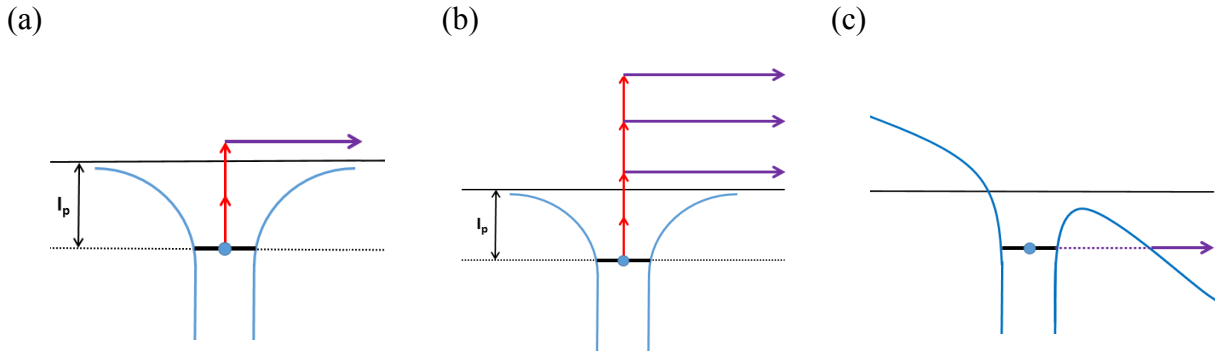

Figure 1.1 Ionization mechanisms. (a) Multiphoton ionization (MPI); (b) Above threshold ionization (ATI); (c) Tunneling ionization (TI);

1.1.3 Keldysh Parameter

To classify the type of strong field ionization, Keldysh defined an adiabaticity parameter, γ, as the ratio of the laser frequency to the tunneling frequency [5]. The Keldysh parameter

provides a useful metric for predicting the likelihood that ionization will occur via tunneling and is defined as,

$$\gamma = \frac{\omega}{\omega_t} = \sqrt{\frac{I_p}{2U_p}}, \qquad (1.3)$$

with ω_t the tunneling frequency. In the high laser frequency limit, where $\gamma >> 1$, ionization only occurs via multiphoton ionization. In the low frequency limit, where $\gamma << 1$, tunneling takes place.

We show the Keldysh parameter for Argon, with I_p=15.6eV, in Table 1.1 for different intensities of an 800nm laser

Intensity(W/cm^2) for 800nm	**U_p(eV)**	**Keldysh parameter**
10^{11}	0.00596	36.3452
10^{12}	0.05965	11.4933
10^{13}	0.59653	3.63452
10^{14}	5.96531	1.14933
10^{15}	59.6531	0.363452

Table 1.1 Ponderomotive energy and Keldysh parameter for Argon at different laser intensities

1.2 High Harmonic Generation

As mentioned above, the other strong field process of relevance for this thesis is high harmonic generation (HHG). HHG can be described as a three step process when using a semiclassical approximation [6, 7]. A cartoon of the three steps of HHG is shown in Figure 1.2. The first step is tunnel ionization, where an electron in the continuum is assumed to be created with zero kinetic energy. After tunnel ionization, the second step is propagation, where the electron is accelerated by the electric field. In this step, the electron is considered to be no longer interacting with the Coulomb field of the parent ion. Finally, when the laser electric field changes direction, the electron is driven back to the parent ion. The returning electron is then recombined with the

parent ion and emits a photon that has energy equal to the ionization potential of the atom plus the kinetic energy of the recombining electron. Under this model, the maximum energy that the electron can acquire through propagation in the laser electric field is $3.2U_p$ [8]. So the maximum energy of the generated photons is $I_p + 3.2\ U_p$ which defines the classical cutoff energy for the emitted harmonic photons.

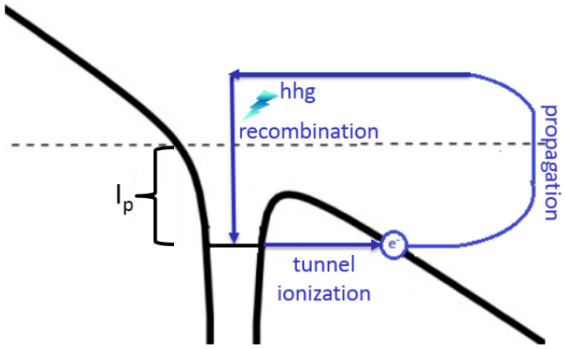

Figure 1.2 Three step model of high harmonic generation

Chapter 2 - Design of Electron Time of Flight Spectrometer

Our design of the Electron Time of Flight (ETOF) spectrometer is based on an electrostatic lens system [9]. The ETOF electrostatic lens system consists of six lenses to reduce chromatic aberration. At the last lens there is a grid to ensure plano convex lens for the collimation of the charged particles. When a dc voltage is applied to an electrostatic lens element the electric field lines form curved equi-potential surfaces that deflect ion/electron trajectories in analogy to ray optics.

2.1 Ion Optics

When a charged-particle beam passes from a region of uniform potential V_1 to a region of uniform potential V_2, as shown in the Figure 2.1, the initial and final kinetic energies of a particle of charge q are $E1=qV_1$ and $E2=qV_2$ respectively. If α1 and α2 are the angles of incidence and refraction with respect to the normal to the equipotential surfaces that separate the field-free regions [10], the charged-particle analog of Snell's law is

$$\sqrt{E_1}\mathrm{Sin}\alpha_1=\sqrt{E_2}\mathrm{Sin}\alpha_2 \qquad (2.1)$$

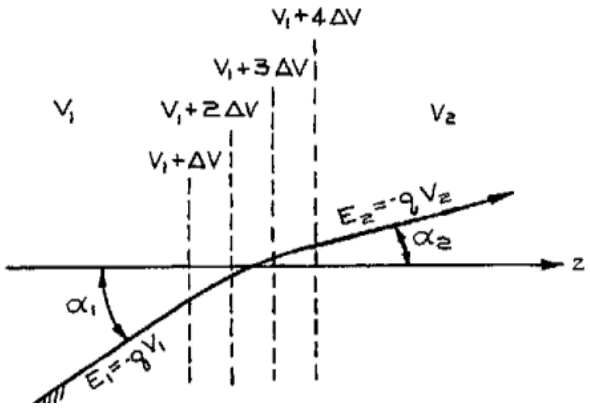

Figure 2.1 A charged-particle trajectory exhibits ''refraction'' at a potential gradient [10].

2.2 SIMION Simulation of ETOF

SIMION is a software package primarily used to calculate electric fields and the trajectories of charged particles in those fields when given a configuration of electrodes with voltages and

particle initial conditions. Field configurations can include optional RF (quasistatic), magnetic field, and collisional effects [11].

The design of the electrostatic lens system of the ETOF is shown in Figure 2.2. The geometry code for the design is listed in Appendix A - .

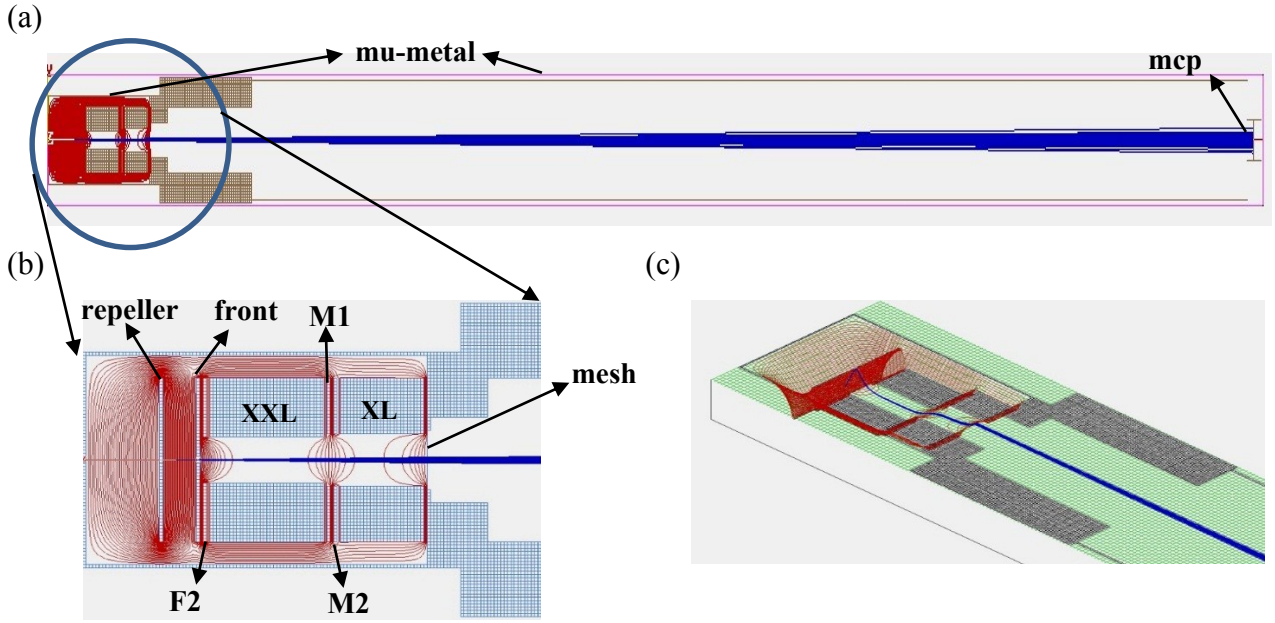

Figure 2.2 (a) SIMION geometry design of our ETOF (b) Lens system of ETOF (c) Acceleration and retardation area due to field lines

The repeller is 1mm thick with no hole, the front electrode is 1 mm thick with 3mm diameter hole, F2 is 1 mm thick with 14mm diameter hole, XXl is 34 mm thick with 15mm diameter hole, M1 is 1 mm thick with 16mm diameter hole, M2 is 1 mm thick with 16mm diameter hole, XL is 25 mm thick with 17mm diameter hole, final plate with mesh is 1 mm thick with 18mm diameter hole. The repeller is separated from the front plate by a Teflon spacer of 10mm. To prevent space charge accumulation, the spacers are coated with a conducting silver paint. Other lenses are separated from each other by 1mm Teflon spacers, with a larger inner hole to prevent charged particles from accumulating on the spacers.

The copper mesh in the last lens has 85% transmission efficiency and is shown in Figure 2.3(b). If the mesh is not used, field lines will be equivalent to a bi-convex optical lens which will diverge the electrons as shown in Figure 2.3(a). With the mesh placed at the last electrostatic lens

the field lines are equivalent to a plano-convex optical lens that collimates the electron to the detector as shown in Figure 2.3(b).

(a) (b)

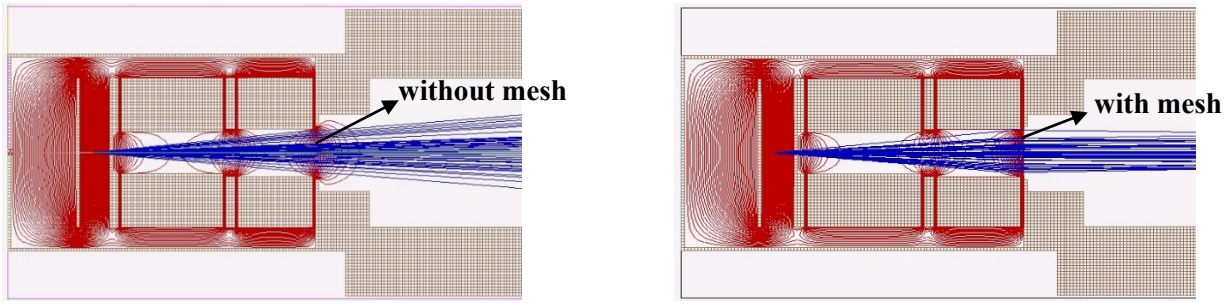

Figure 2.3 Comparison of the immediate electron trajectory after exiting the lens system a) with a biconvex setup (no mesh) and b) with a planoconvex setup (using a mesh).

2.3 Sequential search of optimized voltages in SIMION

In SIMION one can manually adjust the voltages of the electrodes and simulate the path of a charged particle going through the system so as to determine the of trajectory, time of flight and efficiency on the detector for a large number of particle initial energies and angles. To do this manually would be quite tedious; hence a lua sequential search code. Lua is the main programming language supported in and embedded inside SIMION for simulating charged particles programmatically. The lua code sequentially changes the voltages of each lens element for a wide range of particle energies and angles. Efficiency is defined as the ratio of particles that were originally generated to the number of particles that make it to the detector, as defined in Eq. 2.2. The detector is represented by a circle of the same area as the MCP used in the experiment. The code is listed in Appendix B . The sequential search for lens XL and XXL, putting other lens at ground, was carried first (manual adjustment gave the idea that they are crucial lens). In Figure 2.4 we show the electron collection efficiency as a function of XL and XXL voltages. Red values represent a better efficiency, while blue values show a lower efficiency.

$$\text{efficiency} = \frac{electrons\ that\ hit\ on\ the\ detector}{total\ number\ of\ elctrons}\ X\ 100\% \qquad (2.2)$$

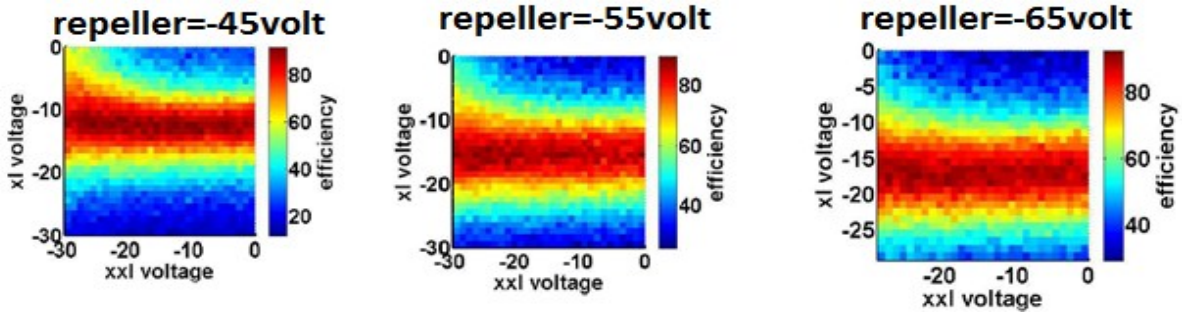

Figure 2.4 Efficiency on the detector for different repeller voltages as function of lens voltages on XXL and XL. Red values represent higher efficiencies while blue values are voltage combinations of low efficiency.

From the Figure 2.4 it is clear that as the magnitude of the repeller voltage is increased the magnitude of XL voltage needs to be increased to maintain a high efficiency. Also, it is apparent that the magnitude of XXL voltage has a large range of values over which the efficiency is maintained. This means that the efficiency is largely independent with the XXL voltage. These results need to be tested in real experiments.

2.4 Design

The ETOF design is shown in Figure 2.5. It consists of the lens system as discussed in section 2.2. All the parts of lens were made of MIC-6 Aluminum. Because of the position of the lens system, it behaves as differential tubing in between the source chamber and the drift tube. The drift tube is of 1m in length and there is an MCP detector at the end of it. The entire lens system and drift tube are shielded with mu-metal to lower the magnetic field. The lens system is put into a 6 inch cross which is pumped with a turbo pump and we get minimum pressure of 6e-9 torr. The drift tube is also pumped with a turbo and the minimum pressure is 5e-8 torr. All the vacuum parts are Conflat based and the material used is nonmagnetic. The Teflon spacer separating the repeller and entrance plate as well as the gas jet needle of inner diameter 200 μm are coated with conductive silver coating to prevent charge build-up.

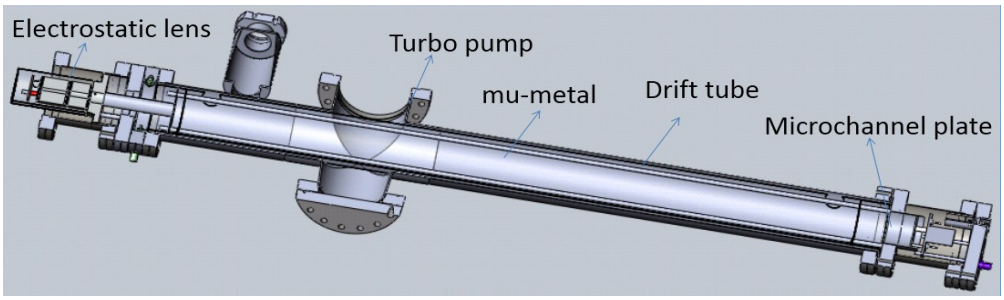

Figure 2.5 Solidworks drawing of ETOF

2.5 Closed loop Experimental Setup

Details of the experimental setup are shown in Figure 2.6. The laser is focused in the interaction region of the ETOF between the repeller plate and the entrance plate. In the experiment, laser intensity is controlled with a half wave plate and polarization cube so as to preserve the pulse duration and spot size for all values of energy. The polarization cube also determines s- or p-polarization. The extra half wave plate after the cube is used for fine tuning of the polarization. The laser is horizontally polarized (perpendicular to the MCP detector) so as to maximize the yield of electrons. A transform-limited pulse in the interaction region is obtained by compensating the group velocity dispersion of the optical elements in the beam path by adjusting the grating pair relative distance in the amplifier compressor. The gas sample is introduced in the interaction region through a glass needle of inner diameter 200μm. The electron or ion generated due to laser interaction with the gas sample is directed towards the MCP detector. In the case of very low energy electrons, the repeller helps to push the electrons/ions towards the detector. As discussed before, the lens system helps in collimating the electrons/ions. We use an oscilloscope to record the time of flight of the electrons/ions. The time spectrum can then be converted to m/q (in case of ions) and energy (in case of electrons). The data acquisition system is completely automated using a LabView interface with the half wavelplate rotation stage, oscilloscope, voltage power supplies to the lens system, and pressure gauges. Once the energy of the laser pulse is stabilized, the laser peak intensity can be calculated by measuring the pulse duration, and the spot size. In our experiments we used a home-built second harmonic generation frequency resolved optical gating (SHG-FROG) to measure the pulse duration and a Mightex camera with a pixel size of 2.5 μm to measure the spot size.

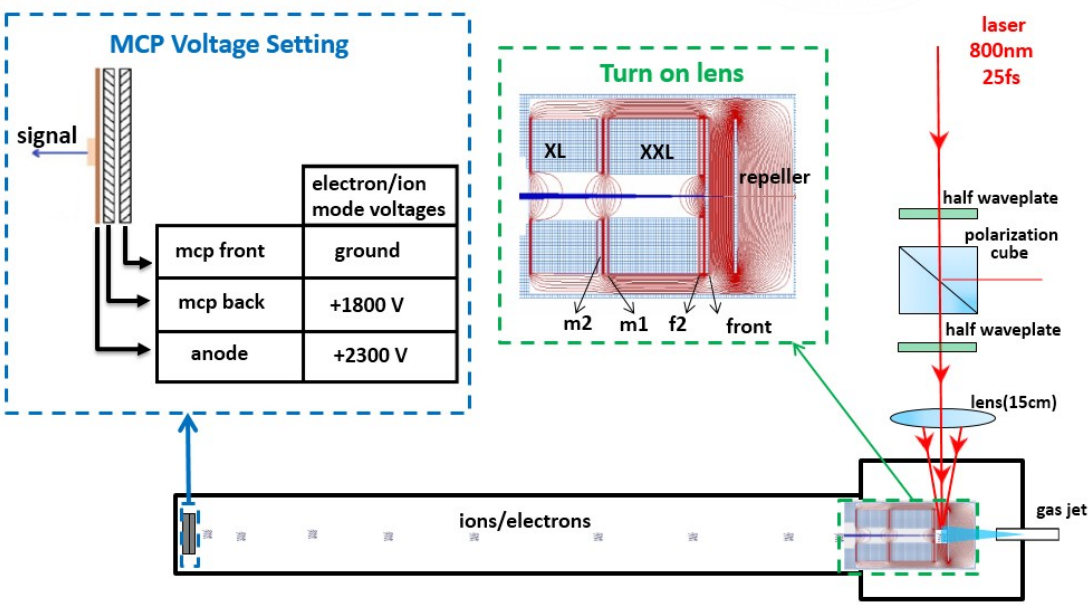

Figure 2.6 Closed Loop Experimental Set-up

(a)

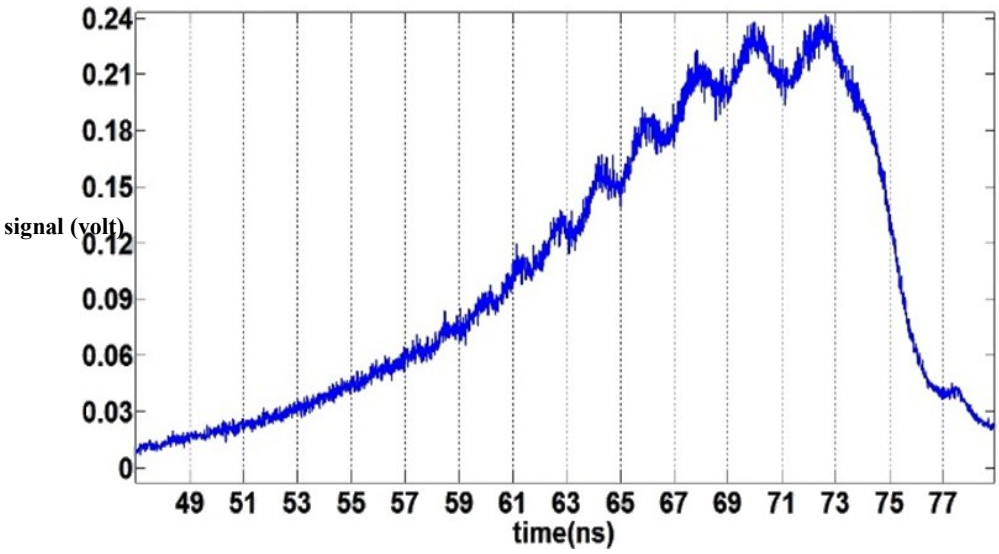

Figure 2.7 ATI electron time-of-flight spectrum of Argon obtained with the experimental setup shown in Fig. 2.6. The lens configuration used is repeller= -50 V, XL= -15 V, XXL = -10V. For this spectrum, an ETOF of length 445cm was used.

A typical ATI electron time-of-flight spectrum of Argon is shown in Figure 2.7. The spectrum was taken with 800 nm, 30 fs laser, with 50μJ energy and Ar pressure of 2e-7 torr.

Chapter 3 - Optimization of Electrostatic Lens of ETOF

3.1 Sequential Search of Electrostatic Lens Voltage

Results of the sequential optimization search in SIMON motivate us to test the same approach experimentally. This can be achieved by programmatically changing the voltages in the lens system and recording integrated yields on the detector. The experimentally obtained results for the sequential optimization are shown in Figure 3.1. Our results show the same trend in the yield as a function of XL lens voltage compared with the simulation results. However, our results are a bit different for the XXL lens voltage as compared to that of sequential optimization in SIMION. For the experiments, just as in the simulations, the other lens voltages were grounded. Only the lenses XL and XXL were considered for tuning as they are crucial for maximizing the yield at the mcp detector. Considering all lenses at once would be too time consuming.

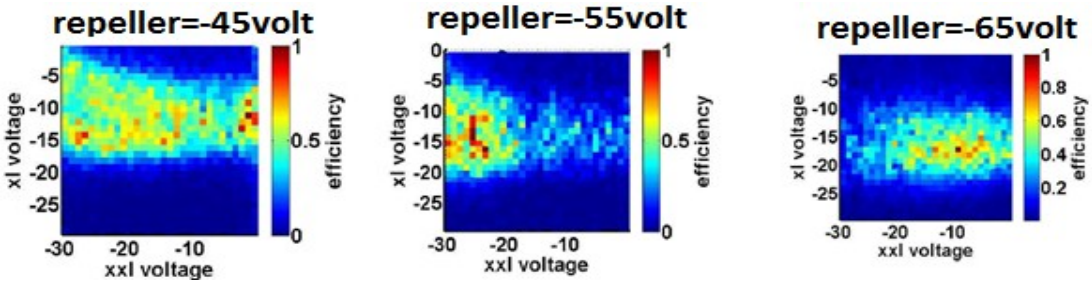

Figure 3.1 Electron yield as function of lens XL and XXL voltages at different repeller voltages

3.2 Genetic Algorithm

The sequential search method is time consuming for maximizing the yield if we want to use all five lenses since the search space becomes too large. For this reason, we used a genetic algorithm (GA) for optimization. A GA is a search techniques inspired from the biological process of evolution by means of natural selection [12, 13]. They can be used to construct numerical optimization techniques that perform robustly on problem characterized by large and complex search spaces.

GA's work by testing the fitness of a population of individuals. Each individual is made out of genes which are manipulated to improve the fitness. Once the fitness of a population is measured,

the genes are manipulated and a generation is formed. With the best individuals of the population, a new generation is formed. Individuals some times are also referred to as chromosomes.

A GA starts with a random population and choosing *random* values for all model parameters. Then:

1. Evaluate the goodness of fit ("fitness") of each member of the current population.
2. Select pairs of solutions ("parents") from the current population, with the probability of a given solution being selected made proportional to that solution's fitness.
3. Breed the two solutions selected in (2) and produce two new solutions ("offspring").
4. Repeat steps (2)–(3) until the number of offspring produced equals the number of individuals in the current population.
5. Use the new population of offspring to replace the old population.
6. Repeat steps (1) through (5) until some termination criterion is satisfied or stop when the fitness is optimized.

These can be shown by flow chart in Figure 3.2.

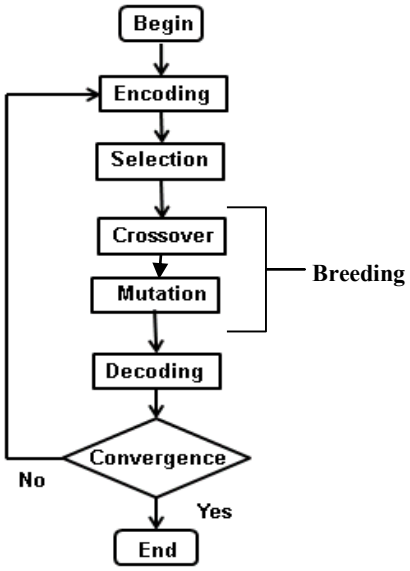

Figure 3.2 Flow Chart for GA

In the flow chart, encoding is the method of changing the GA parameters into chromosomes (one column array of decimal digits) to form the individual and the decoding is the reverse of it.

Cross over is the interchange of certain part of a chromosome between two chromosomes from particular point called locus. Mutation is a slight change in the chromosome value at a certain point only [12, 13].

3.2.1 Theoretical GA

GA's are largely divided into two categories; micro-GA and regular GA. A micro GA is a GA where the population size is very small (less than ten individuals) whereas usual population size is of 20 or higher. Micro-GA's are usually used for small search spaces like ours. Therefore, we theoretically investigated the speed and robustness of both approaches. Speed is measured in the total number of evaluations needed to converge to a solution. The number of evaluations is the relevant quantity in our case since measuring an electron TOF spectrum is time consuming. For this reason, we require that the GA converges to a solution by measuring as few spectra as possible.

We employed a LabView based GA library named Waptia [14]. Waptia GA consists of different reproduction plans and mutation plans and is based on a well-known Fortran set of routines. We start by defining a five-dimensional Gaussian fitness function with different mean and standard deviation (Eq. 3.1). In Eq. 3.1 a random noise is fed into the Gaussian fitness function so as to simulate real experimental scenario.

$$Fitness = e^{-\sum_{i=1}^{5}\left(\frac{x_i-\sigma_i}{\mu_i}\right)^2} + noise \qquad (3.1)$$

$$noise = (0.5\text{-random number } (0, 1))*\text{error percent} \qquad (3.2)$$

We carried on optimization by beginning the GA with a population size of 5 individuals (micro GA) and 20 individuals (GA). It is found that for all kinds of reproduction plans and mutation plans, the total number of evaluations required to converge for the regular GA is better than that for a micro-GA.

a)

Parameters	Micro GA	GA
Population size	5	20
generations	400	100
Significant digits	2	2
Crossover probability	0.5	0.85
Mutation Rate	0.04	0.08

b)

Reproduction Plans	Mutation Plans
Full generation replacement (elitism)	One point, fixed rate mutation
Steady state replace random	One point, fitness adjustable rate
Steady state replace worst	One point, distance adjustable rate

Table 3.1 a) Parameters used for Micro GA and GA. Generations indicate the maximum number of generations used. The mutation rate and crossover probabilities are lower for a micro-GA to guarantee convergence b) Reproduction plans and mutation plans used.

We tested both the GA and micro GA with the parameters shown in Table 3.1 a) for all possible combinations of the reproduction plans and mutation plans mentioned in Table 3.1 b) (9 possible plans). We found that full generation replacement reproduction and fixed rate mutation was the best combination for optimization. The maximum total number of generations is chosen such that both GA implementations have the same total number of evaluations. Also, because the micro-GA has such a small population the mutation rate and crossover probabilities can't be too large in order to achieve convergence.

(a)

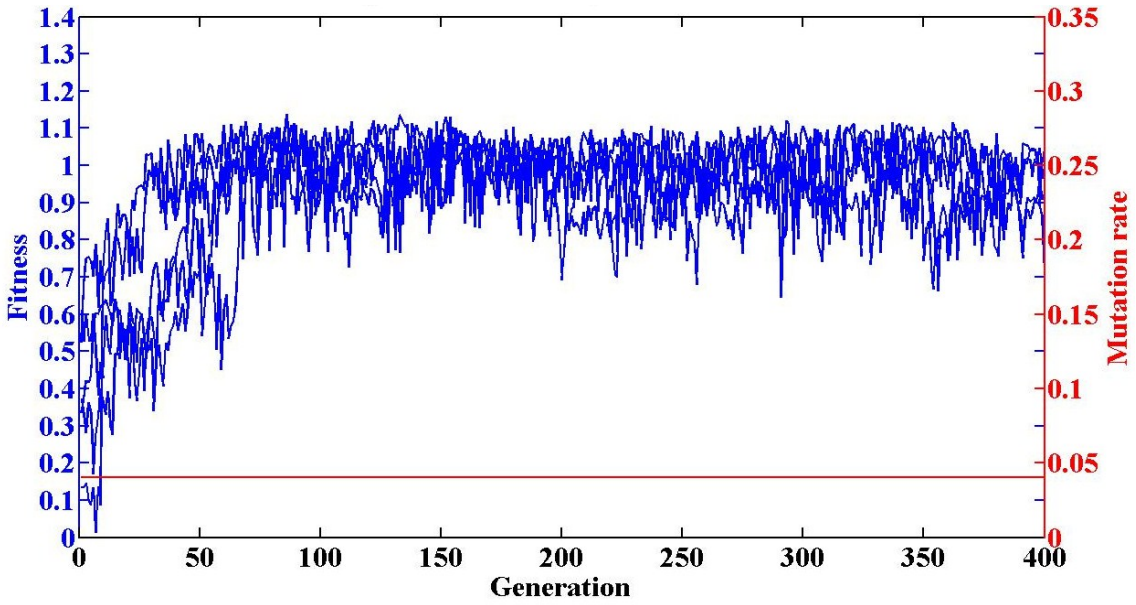

(b)

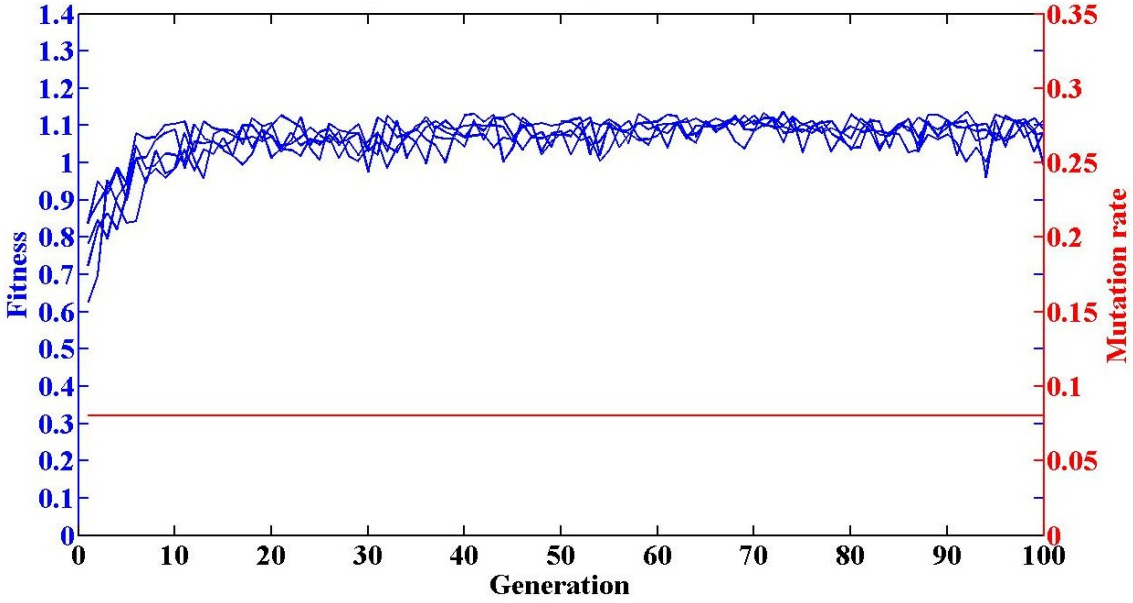

Figure 3.3 Fitness as a function of generation for a) Micro GA b) GA. Each line in both graphs represent a different "run". Shown is the best individual of each generation. Noise level was set at 20% for all cases.

Figure 3.3 shows the fitness as a function of generation for (a) micro-GA and (b) GA with 20% noise as defined in Eqs. 3.1 and 3.2. Each line in the graph represents a different run and deviations from run to run show the robustness of the method. From the figure it can be seen that

the conventional GA consistently optimizes around the 10th generation with 20X10=200 evaluations. On the other hand, the micro-GA is quite inconsistent in the number of generations needed to achieve convergence. The micro-GA optimizes at the 30th to 75th generation with 30X5=150 to 75X5= 375 evaluations. Hence our theoretical studies show that the total number of evaluations for a normal GA is less and more consistent compared to micro- GA. For both GA's the full generation replacement reproduction plan and fixed rate mutation were the optimum settings. So we used a GA with conventional population size of 20 individuals, and full generation replacement reproduction plan plus fixed rate mutation in the experiments.

In addition, we also studied the effect of noise on the results by the GA. Most notably, when noise is added to the GA the fitness dependence with generation is not smooth. This is due to the fact that the fitness of each individual will be affected by the experimental error and thus, the optimal individual might appear as not-optimum in the presence of noise. This is shown in Figure 3.4, where the fitness as a function of generation is shown for different noise levels.

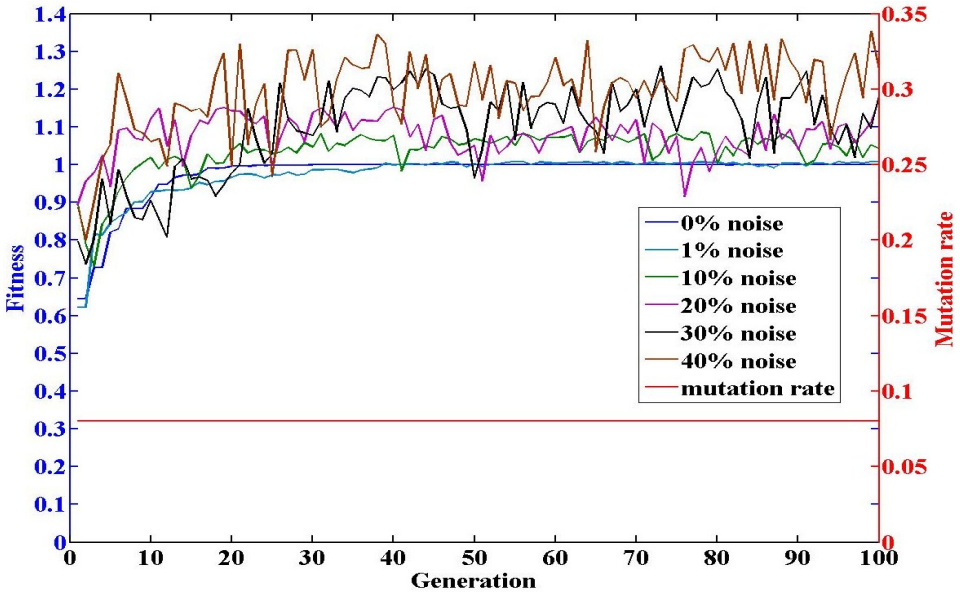

Figure 3.4 Theoretical GA with different noise levels

3.2.2 Experimental GA

The translation of the GA language to our experiment is as follows. Genes are the individual lens values up to two significant digits. Individuals are defined as the combination of lens voltages. Fitness is the total (integrated) yield on the detector. To account for experimental sources of noise fitness values are "penalized" in the presence of non-ideal experimental

conditions. Thus, the electron yield (fitness) is divided (penalized) by the shot-to-shot measured laser power and the measured pressure of the gas in the interaction region (Eq. 3.3). This penalization guarantees that individuals do not acquire a better fitness due to experimental fluctuations. It should be mention that while this is a good approximation for the pressure, it is not a good approximation for the laser power fluctuation. The reason for this is that while the electron yield is directly proportional to the pressure, it is obviously not a linear function of laser power (peak intensity). For this reason, we further discriminate the fitness with respect to laser power. To do this, we measure the single-shot laser energy and calculate the deviation with respect to the initial measured valued of the energy. If the fluctuation in power (Eq. 3.4) is larger than a preset limit for the energy fluctuation (typically 1%) then the trace is discarded.

$$\text{Fitness} = \frac{Total\ Yield}{Pressure * Power} \tag{3.3}$$

$$\%\ \text{Error in Power} = \frac{Initial\ Power - Current\ Power}{Initial\ Power} X100 \tag{3.4}$$

Because the measured yield is recorded as a function of time, we choose an integration window such that the photo electron spectrum is within that window for all possible lens values. Also, the repeller voltage is the same for a particular lens voltage optimization. Note that the lens voltage alteration has nothing to do with an overall shifting of the photoelectron spectrum, only altering the repeller voltage completely shifts the photoelectron spectrum. This last statement has been demonstrated by both SIMION simulations and experimental measurements. Our GA is started with population size 20 with full generation replacement reproduction plan and fixed rate mutation as suggested from the theoretical GA. The initial population is chosen to be centered around the optimized lens values given by our SIMION optimization.

a)

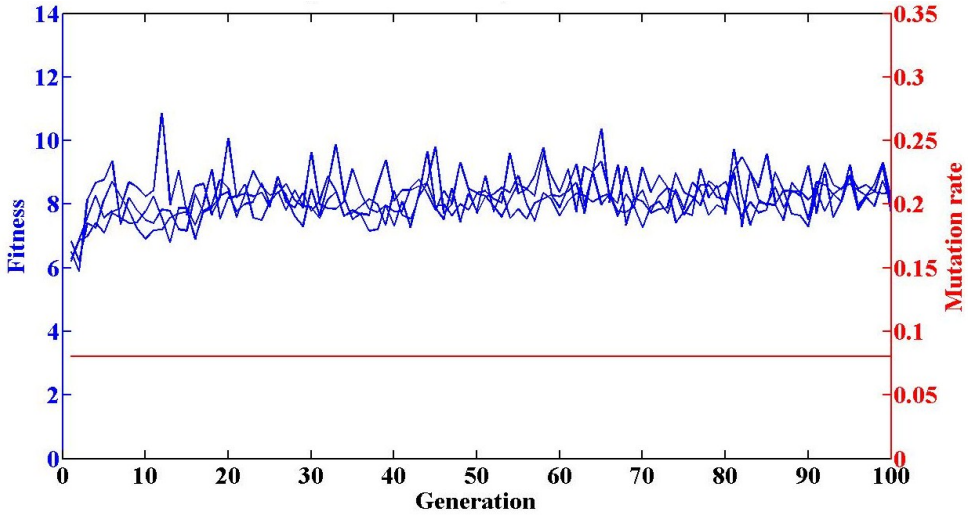

b)

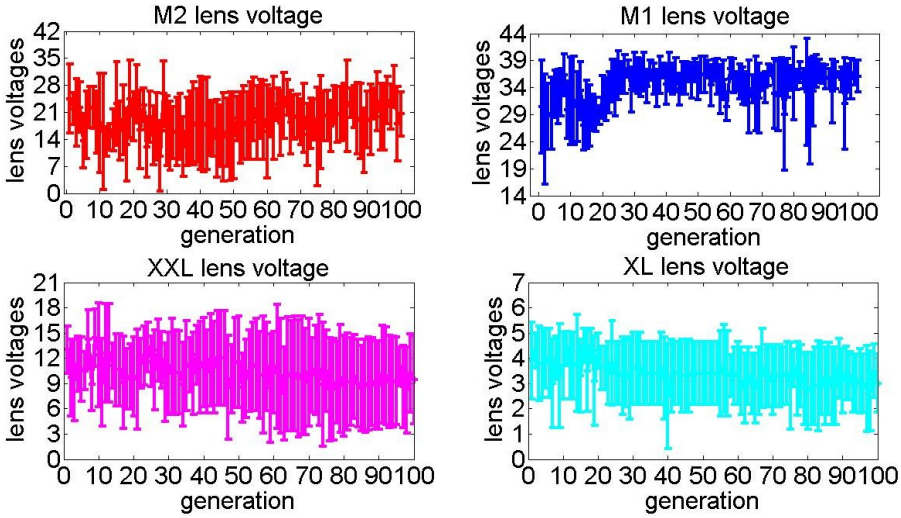

Figure 3.5 (a) Experimental fitness as a function of generation for the GA without power discrimination repeated 4 times, (b) lens voltages obtained as a function of generation, with error bars, for case (a). The error bars are measured as the standard deviation from the 4 runs.

A summary of the experimental optimization results is shown in Figure 3.5. In addition to the results shown, it was found that the F2 lens had no impact on the yield of the photo electron so it is eliminated from the GA. Panel a) of the figure shows the fitness as a function of generation for four different runs using 800nm, 30 fs pulses and 1% power discrimination. From the figure it is clear that the improvement in the electron yield is not large, and the algorithm converges after

10 generations. It is further seen that the XL lens is the most crucial lens since the value of the voltage for XL changes following the fitness function. On the other hand, XXL, M1, M2 do not have a large impact on the overall fitness as can be seen by the large distribution in their values. This large distribution indicates that there are a large set of voltage values for XXL, M1, and M2 that will maximize the electron yield.

We observed no difference in the GA solutions with and without power discrimination at 800nm. This is due to the fact that the laser fluctuations are <1%. We expect that power discrimination will have a larger impact on OPA generated photo electrons

3.2.3 Comparison of Sequential Search (SIMION and Experiment) and GA

In Table 3.2we show the optimized voltages of the electrostatic lenses for all the employed methods of optimization.

Method	repeller	F2	XXL	M1	M2	XL
GA	-35 volt	0	-4 volt	-34volt	-21 volt	-9 volt
Sequential search	-35 volt	0	-2 volt	0	0	-10 volt
SIMION	-35 volt	0	-17 volt	0	0	-11volt

Table 3.2 Lens Voltages for GA, Sequential Search and SIMION

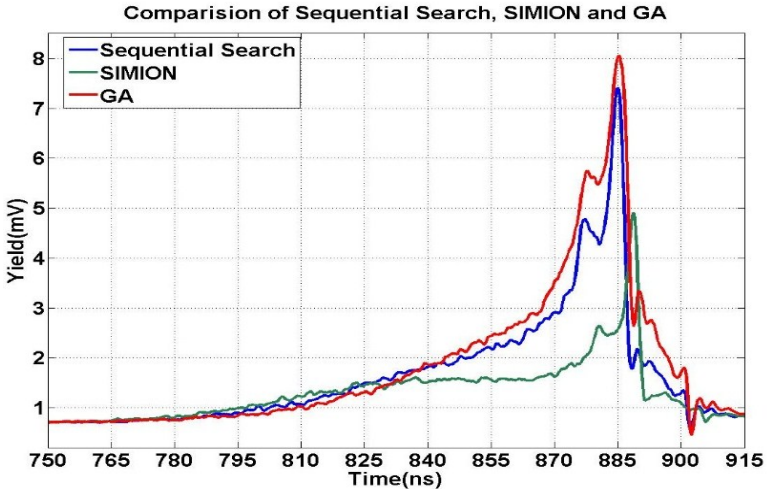

Figure 3.6 Comparison of experimentally measured electron yield for experimental sequential search (blue), experimental GA (red), voltages suggested by the SIMION sequential search (green)

In Figure 3.6 we show the experimentally obtained photoelectron spectrum using lens voltage configurations obtained with the GA (red), sequential search (blue) and the SIMION optimization (green). The figure demonstrate that the yield is maximum with the GA-obtained optimization. However, it is also clear that the voltage configuration for the GA is shifting the high energy electrons as well as the relative contribution of the low-energy electrons. Still, we have demonstrated that the GA is the quickest method for optimization and does provide an improvement in the overall signal.

Chapter 4 - Conclusion and outlook

4.1 Outlook: Towards the characterization of attosecond pulses

One of the main topics of research in our group is the generation of XUV pulses by HHG and its subsequent characterization. One consistent issue with the characterization of HHG pulses is that they have a very low flux. Therefore, one of the first steps was to work towards the generation of brighter XUV pulses. My approach was to build a semi-infinite gas cell. The basic idea is that when a laser is loosely focused with a long focal length lens, there is an enhancement in the HHG process due to a larger interaction region of the laser with the gas [15]. Other approaches used in our group make use of a two color field (ω/2ω) field to drive the HHG. In this case the yield will increase as the laser field is sculpted in such a way that short trajectories are dominant compared to long trajectories producing high yield HHG [16].

Figure 4.1shows the experimental setup for the generation of harmonics using a semi-infinite gas cell. The inset shows a typical HHG spectrum generated with the semi-infinite gas cell. While work is still undergoing to fully characterize the cell, it was clear that the cell can generate much brighter harmonics than the standard gas jet.

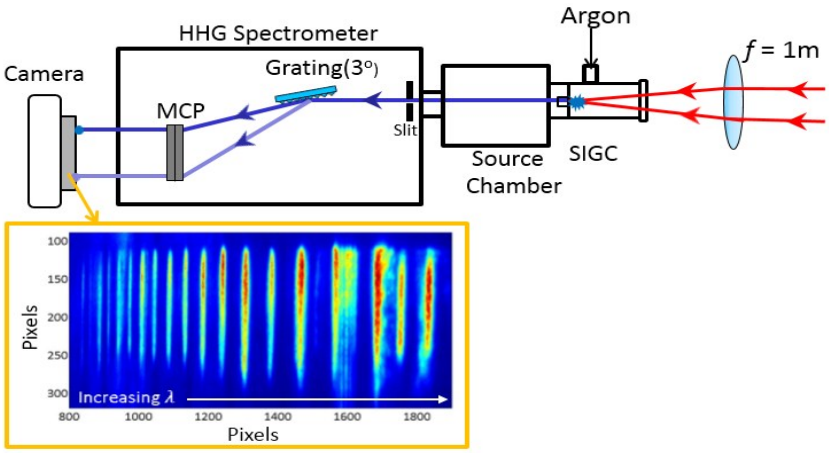

Figure 4.1 Experiment Set-up for High Harmonic generation in semi-infinite gas cell.

4.1.1 Reconstruction of Attosecond Beating by Interference of Two Photon Transition (RABITT)

Spectrally, HHG produces photons that are separated by 2ω. In the single-photoionization process of noble gas atoms by spectrally and temporally filtered extreme ultraviolet (XUV)-attosecond pulse train (APT), the measured electrons exhibit kinetic energies, which are separated by 2ω, thus reflecting the corresponding high harmonic photon energies. By simultaneously irradiating the atoms with a moderately intense IR field, sidebands peaks will appear in the electron energy spectrum. For each sideband there are two indistinguishable contributions, or quantum paths. One path comes from the absorption of an IR-photon together with a primary XUV harmonic transition (q-1), and the other corresponds to the emission of an IR-photon from the consecutive primary XUV harmonic transition (q + 1) (see Figure 4.2). The basic idea of RABITT is that phase information can be extracted from the sideband oscillation as the XUV and IR pulses are delayed [17].

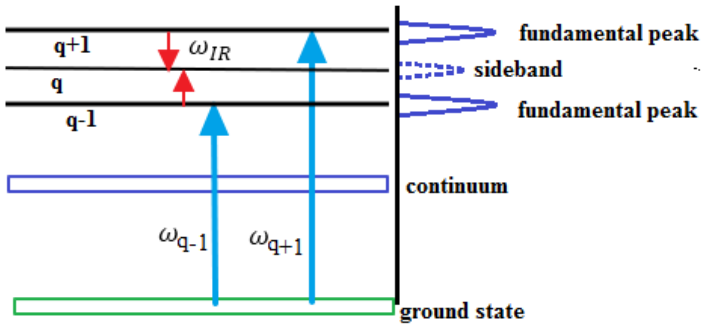

Figure 4.2 Spectral scheme of RABITT

The phase of the sideband is given by,

$$\phi_{SB}(\omega_q) = \varphi(\omega_{q+1}) - \varphi(\omega_{q-1}) - \Delta\varphi_q^{at} \approx 2\omega_0 t_e(\omega_q) \qquad (4.1)$$

where $\Delta\varphi_{q+1}^{at}$ (the atomic phase term) is only a small correction. Sideband phase oscillation $\phi_{SB}(\omega_q)$, which is observed in the experiment, gives the relative phase of consecutive high harmonics.

4.1.2 RABITT Experimental Setup

To build a RABITT setup we need to send the XUV radiation into our ETOF and recombine it with IR pulses. The RABITT experimental system is shown in Figure 4.3, it consists mainly three regions; generation of harmonics, XUV spectrometer and ETOF.

Optically, the incoming IR beam is divided into two arms with a beam splitter. One arm is focused into a gas jet in the high harmonic chamber. The generated harmonics co-propagate with the fundamental which is filtered. The XUV beam is focused into the gas jet in the ETOF with a toroidal mirror (TM) followed by a flat mirror (FM). The FM has two purposes, first it redirects the XUV beam in a straight line i.e. parallel to the initial direction before the toroidal mirror and second it eliminates 80% of the fundamental beam by absorption. To further filter the fundamental beam we use an Al filter. The toroidal mirror has a focal length of 40 cm such that we have a 2f-2f imaging setup for the XUV (i.e 80cm-80cm). This means that we will have a one-to-one imaging in the ETOF of the generated harmonics at the first gas jet. The IR beam on the other arm is focused to the detection gas jet in ETOF by a 15 cm focal length off-axis parabolic mirror. The peak intensity of the IR generating the harmonics should be much stronger than the IR beam sent into the ETOF [18].

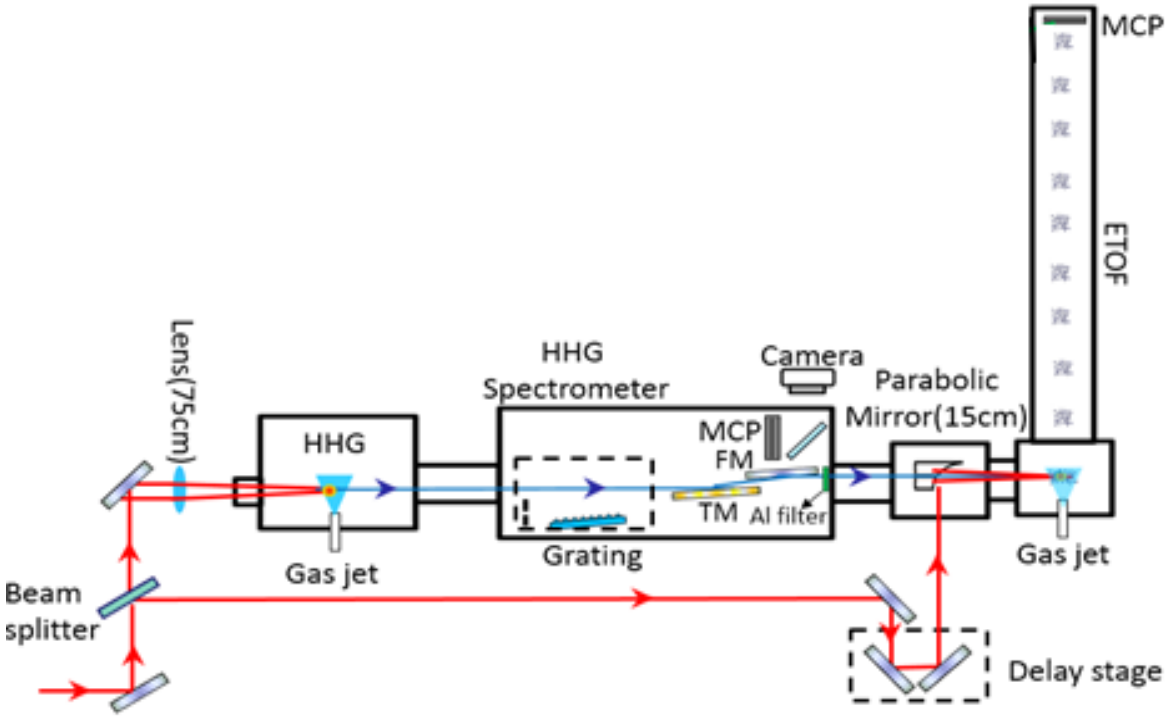

Figure 4.3 Experimental Set-up for RABITT

4.1.2.1 Toroidal Mirror(TM)

The toroidal mirror (Figure 4.4) is a gold reflective mirror specially used for XUV at glancing incidence so that reflection efficiency is high. TMs' are focusing devices having two different radii whose axes are oriented perpendicularly. They are utilized in instances where a beam must be focused and folded. Rather than using both a spherical mirror and a plane mirror for this purpose, both functions may be combined in one element. Toroidal mirrors also correct for the astigmatism that result when a spherical mirror is used off axis [18].

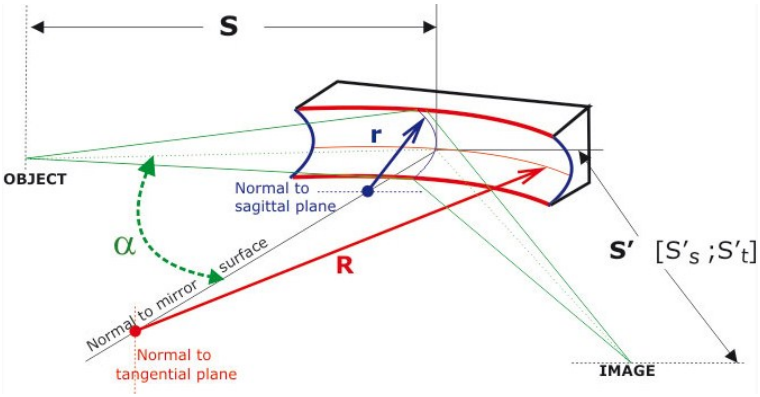

Figure 4.4 Toroidal Mirror with Sagital and Tangential plane parameters [18]

$$\frac{1}{S}+\frac{1}{S_s'}=\frac{2Cos\alpha}{r} \qquad (4.2)$$

$$\frac{1}{S}+\frac{1}{S_t'}=\frac{2}{RCos\alpha} \qquad (4.3)$$

α – the angle of incidence (to Normal); one half the included angle of the incident and reflected rays;

S – Object conjugate distance; **S'** – Image conjugate distance;

S'$_s$ – for the sagittal plane; **S'$_t$** – for the tangential plane;

r – the Radius whose axis of revolution is oriented **in the sagittal** plane; also called the cylinder curve.

R – the Radius whose axis of revolution is **in the tangential** plane; also called the base curve.

For our TM setup, we chose the object/image distance to be **S= S'$_t$ =S'$_s$=** 80 cm. We also used α = (90-4) =86^o since the angle of incidence to the plane of TM is 4^o to maximize the reflectivity of the XUV beam on gold.

With these consideration we obtain the radius whose axis of revolution is oriented **in the sagittal** plane as

$r = \frac{S}{\cos\alpha} = \frac{80cm}{\cos 86^o}$ =1146.846cm,

And the radius whose axis of revolution is **in the tangential** plane as

R= S$\cos\alpha$ = 80cm * $\cos 86^o$= 5.585cm

Hence our gold coated TM with surface roughness <10 angstroms, for XUV radiation at an incidence angle of 4º to the plane, should have a sagittal plane radius of 1146.85 cm and a tangential plane radius of 5.58 cm [Appendix C -].

4.1.2.2 Off-Axis Parabolic Mirror with hole

To recombine the XUV and the IR in the ETOF we used and off-axis parabolic mirror with a hole in the center. It is used for focusing the IR into the interaction region in the ETOF while the XUV passes through the hole in the center. We used an off-axis parabolic mirror with a hole from Thorlabs with focal length of 6 inches and a conical hole of 8mm on front and 3mm on back. The hole through which XUV passes should be big enough such that the XUV is not clipped. Our simple arithmetic calculation taking the XUV spot size at the TM to be 12mm shows that it won't clip while passing through the parabolic mirror.

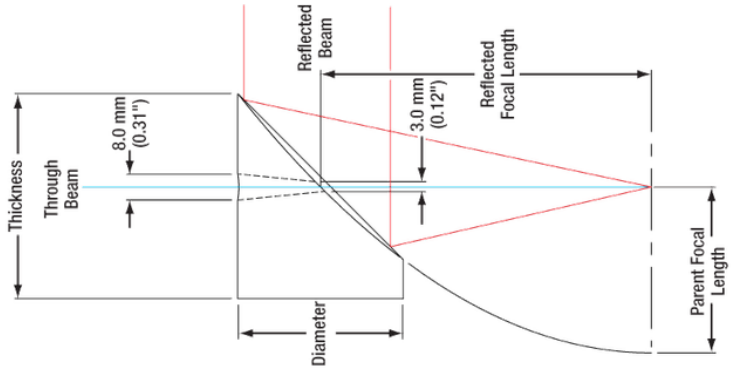

Figure 4.5 Off-axis Parabolic Mirror with hole used to recombine the IR and XUV pulses for RABITT experiments [20]

At the time of this thesis, the system was assembled but we had not been able to measure electrons from the XUV pulses.

4.2 Conclusion

We built an electron time-of-flight spectrometer with a flexible electrostatic lens system to measure photoelectrons up to 150 eV. The ETOF also has a repeller that can be used to measure low-energy electrons as well as ions. For both ions and electrons, the ETOF was simulated, characterized and calibrated using SIMION. For electrons, we have preliminary results showing ATI peaks when using 800 nm pulses. In order to optimize the yield of the detected electrons we theoretically (SIMION) and experimentally optimized the lens system. Experimentally we used a closed loop system that dynamically controls the voltage applied to the lenses. The closed loop was driven by a sequential search and by a genetic algorithm (GA). The GA was found to be the quickest optimization algorithm and to give a higher yield when compared to the voltages simulated in SIMION and the sequential optimization. However, the voltages applied to the lens distorted the obtained spectrum. Regarding the GA, we found that full generation replacement reproduction plan and fixed rate mutation was the best combination for optimization. Also, we found that a GA with a large population size converges to an optimized solution more reliably and, in average, faster than a micro-GA. Finally, the design of all the necessary optics to complete the RABITT experiments was done. The ETOF is joined to the working HHG spectrometer with all optics necessary for RABITT experiments installed.

References

1. K.F.WallandA.Sanchez, Titanium Sapphire Lasers, The Lincoln Laboratory Journal Volume 3. Number 3. 1990

2. Agostini P et al, Free-Free Transitions Following Six-Photon Ionization of Xenon Atoms, Phys. Rev. Lett. 42 1127(1979)

3. R. R. Freeman, P. H. Buckbaum, H. Milchberg, S. Darack, D. Schumacher, and M. E. Geusic, Above-Threshold Ionization with Subpicosecond Laser Pulses, Phys. Rev. Lett. 59, 1092 (1987).

4. Ammosov V M, Delone N B, Krainov V P, Tunnel ionization of complex atoms and of atomic ions in an alternating electromagnetic field , Sov. Phys. JETP 64 1191 (1986)

5. L.V.Keldysh, Ionization in the Field of a Strong Electromagnetic Wave, Sov. Phys. JETP20, 1307 (1965).

6. J. L. Krause, K. J. Schafer, and K. C. Kulander, High-order harmonic generation from atoms and ions in the high intensity regime, Phys. Rev. Lett. 68, 3535 (1992).

7. M. Lewenstein, Ph. Balcou, M. Y. Ivanov, A. L'Huillier, and P. B. Corkum, Theory of high -harmonic generation by low-frequency laser fields, Phys. Rev. A 49, 2117 (1994).

8. P. B. Corkum, Plasma perspective on strong field multiphoton ionization, Phys. Rev. Lett. 71, 1994-1997 (1994)

9. A. Paulus et al., Novel time-of-flight electron spectrometer optimized for time-resolved soft-x-ray photoelectron spectroscopy, Rev. Sci. Instrum. 77, 043105 (2006).

10. Building Scientic Apparatus, Jul 20, 2009 by John H. Moore and Christopher C. Davis.

11. http://simion.com/info/demotour.html.

12. Charbonneau, P., and Knapp, B. 1995, A User's guide to PIKAIA 1.0, *NCAR Technical Note 418+IA* (Boulder: National Center for Atmospheric Research).

13. Davis, L. 1991, Handbook of Genetic Algorithms (New York: Van Nostrand Reinhold).

14. https://lavag.org/files/file/94-waptia-genetic-optimization-algorithm/.

15. J. R. Sutherland, E. L. Christensen, N. D. Powers, S. E. Rhynard, J. C. Painter, and J. Peatross, High harmonic generation in a semi-infinite gas cell, Optics Express Vol. 12, Issue 19, pp. 4430-4436 (2004).

16. Cheng Jin, Guoli Wang, Hui Wei, Anh-Thu Le & C. D. Lin,Waveforms for optimal sub-keV high-order harmonics with synthesized two- or three-colour laser fields , Nature Communications 5, Article number:4003 (2014).

17. Y. Mairesse, A. de Bohan, L. J. Frasinski, H. Merdji, L. C. Dinu, P. Monchicourt, P. Breger, M. Kovačev, R. Taïeb, B. Carré, H. G. Muller, P. Agostini, P. Salières, Attosecond Synchronization of High-Harmonic Soft X-rays, Science 28 Nov 2003:Vol. 302, Issue 5650, pp. 1540-1543.

18. P. M. Paul, E. S. Toma, P. Breger, G. Mullot, F. Augé, Ph. Balcou, H. G. Muller, P. Agostini, Observation of a Train of Attosecond Pulses from High Harmonic Generation, Science01 Jun 2001 : 1689-1692.

19. http://www.lasertechn.com/index.php/toroidal-mirrors.

20. http://www.thorlabs.com/newgrouppage9.cfm?objectgroup_ID=7197.

Appendix A - SIMION Geometry File

```
pa_define(1222,50,1,c,y,e)
        e(1)
        {locate(0)
        {
                fill{within{polyline(0,0,0,33,113,33,113,32,1,32, 1,0)}}
            }
        }
        e(2)
            {
                locate(23)
        {
                        fill{within{box(0,0,1,25)}}
                    }
        }
        e(3)
            {
                locate(34)
            {
                fill{within{box(0,1.5,1,25)}}
            }
            }
        e(4)
            {
                locate(36)
            {
                fill{within{box(0,7,1,25)}}
            }
            }
        e(5)
            {
                locate(38)
            {
                fill{within{box(0,7.5,34,25)}}
            }
            }
                e(6)
            {
                locate(73)
            {
                fill{within{box(0,8,1,25)}}
            }
            }
```

```
e(7)
   {
      locate(75)
     {
      fill{within{box(0,8,1,25)}}
     }
   }

e(8)
   {
   locate(77)
     {
     fill{within{box(0,8.5,25,25)}}
     }
   }

e(9)
   {
      locate(103)
     {
      fill{within{box(0,9,1,25)}}
     }
   }
e(10)
   {
      locate(103)
     {
      fill{within{box(0,0,0,25)}}
     }
   }
e(10)
   {
      locate(103)
     {
      fill{within{polyline(0,12.5, 0,12.5, 0,32,10,32,10,48,18,48, 18,12.5)}
   }}}
e(11)
   {
      locate(121)
     {
      fill{within{box(0,25,83.8,48)}}
     }
   }
e(12)
   {
   locate(1210)
```

```
        {
        fill{within{box(0,0,1,13.5)}}
        }
    }
e(13)
    {
        locate(205)
        {
         fill{within{box(0,44,1000,45)}}
        }
    }
e(14)
    {
        locate(1205)
        {
         fill{within{box(0,14,15,15)}}
        }
    }
```

Appendix B - LUA Sequential Search for Electrostatic lens Optimization

```
================================================================================
    -- This program steps the lens voltages and keep track of the efficiency of electron at the detector and saves lens voltages with respective efficiency
================================================================================
simion.workbench_program()
    --===== variables
    adjustable max_volt_xxl= 0    -- tuning voltage upper bound
    adjustable min_volt_xxl = -31  -- tuning voltage lower bound
    adjustable max_volt_xl= -15    -- tuning voltage upper bound
    adjustable min_volt_xl = -16  -- tuning voltage lower bound
    adjustable max_volt_m1= 0      -- tuning voltage upper bound
    adjustable min_volt_m1 = -1    -- tuning voltage lower bound
    adjustable max_volt_m2= 0      -- tuning voltage upper bound
    adjustable min_volt_m2 = -1    -- tuning voltage lower bound
    adjustable rep = -55
    adjustable particles = 400
    local fh = assert(io.open('rep55_max30_xlxxl.txt', 'a'))
    adjustable step_volt_xxl =1
    adjustable step_volt_m1 = 1
    adjustable step_volt_m2 = 1
    adjustable step_volt_xl = 1
    adjustable run_number = 0           -- rerun counter
    adjustable request_rerun = 1        -- flag: request a rerun
     local update_pe = true             -- mark PE display update at start of each run.
    local num_particles
    --===== subroutines
    -- SIMION initialize segment.  Called on particle creation.
    -- Set initial voltages and control reflying.
    function segment.initialize()
       update_pe = true
       if run_number == 0 then
          xxl = max_volt_xxl
             m1 = max_volt_m1
             m2= max_volt_m2
             xl = max_volt_xl
          rep=rep
       end
       -- If the last run cleared the rerun flag, we'll disable further reruns.
       -- (The current run will still execute.)
       sim_rerun_flym = request_rerun
    end
     -- SIMION fast_adjust segment. Called multiple times per time-step
```

```
-- to adjust voltages.
-- Update electrode voltage.
function segment.fast_adjust()
        adj_elect02 = rep
        adj_elect05 = xxl
        adj_elect06 = m1
        adj_elect07 = m2
        adj_elect08 = xl
end
-- SIMION other_actions segment.  Called on every time-step.
-- Update PE surface display.
function segment.other_actions()
   if update_pe then             -- if update flagged
      update_pe = false
      sim_update_pe_surface = 1       -- update the PE surface display
   end
end
local num_hits=0
function segment.terminate()
filename=tostring(run_number)
   if run_number<10 then
   file =
assert(io.open("J:/pratap_atto_char/tof_imp_sim/finaletof_v4/test/55repxl15xxl0"..filename..".txt
", 'a'))
   else
   file =
assert(io.open("J:/pratap_atto_char/tof_imp_sim/finaletof_v4/test/55repxl15xxl"..filename..".txt"
, 'a'))
   end
   local speed_f = math.sqrt(ion_vx_mm^2+ion_vy_mm^2  )*1000
   local ke_f=0.5*ion_mass*1.66*(10^-27)*(speed_f^2)/(1.60*(10^-19))
   ke_f= tonumber(string.format("%.2f", ke_f))
   y_position=tonumber(string.format("%.2f", ion_py_mm))
   --print(string.format("%.2f, %.2f",ke_f,ion_py_mm))
   file:write(ke_f,'\t',y_position,'\n')
   file:close()
if ion_px_mm >1209 and ion_px_mm <1210 and ion_py_mm >-13 and ion_py_mm <13 then
   num_hits = num_hits + 1
   end
   if ion_number  == particles  then
      local efficiency = 100 * num_hits /particles
      -- display results

         print("n = " .. run_number ..
                  ", xxl = " .. xxl ..
                           ", m1 = " .. m1 ..
```

```
                        ", m2 = " .. m2 ..
                        ", xl = " .. xl..
                        ",efficiency (%)=", efficiency)

        fh:write(xxl,'\t',m1,'\t',m2,'\t',xl,'\t',efficiency,'\n')
    run_number = run_number + 1
    xxl = xxl-step_volt_xxl

    if xxl <= min_volt_xxl then
           xxl=max_volt_xxl
           xl=xl-step_volt_xl
           end
        request_rerun = 1
           num_hits = 0
        end
 if xl <= min_volt_xl then
        request_rerun = 1
        xl=max_volt_xl
        xxl=max_volt_xxl
        m1=m1-step_volt_m1
if m1 <= min_volt_m1 then
        request_rerun = 1
        xl=max_volt_xl
        xxl=max_volt_xxl
        m1=max_volt_m1
    m2=m2-step_volt_m2
if m2 <= min_volt_m2 then
        request_rerun = 0
if  m1 == min_volt_m1 and m2 == min_volt_m2 and xxl ==min_volt_xxl and xl ==
min_volt_xl then
fh:close()
      end
        end
   end
 end
end
```

Appendix C - Toroidal Mirror

Toroidal Mirror is brought from 'http://www.arwoptical.com/' with following specification

Mirror, Toroidal, 25mm x 150mm
400mm FL at 4 degree grazing-incidence

Specifications:

Radii (concave): +/- 1%

Dimensions: +/-0.10mm on L x W and +/-0.15mm on center thickness; CT = 20mm +/- 0.15mm

Coating: Bare gold coating

Clear Aperture: >90% (centered)

Back Surface: fine ground finish

Surface Roughness: < 10 angstroms rms

Material: Pyrex, fine annealed or equivalent

Surface Quality: 20-10 scratch-dig

Protective Chamfers: <0.50mm x 45 degrees